Supporting Information for

Isolating Pure Donor and Acceptor Signals by Polarization-Controlled Transient Absorption Spectroscopy

*Yi Xu[1], Lars Mewes[1], Erling Thyrhaug[1], Vladislav Sláma[2], František Šanda[2], Heinz Langhals[3] and Jürgen Hauer[1]**

[1] Technical University of Munich, TUM School of Natural Sciences, Department of Chemistry, Professorship of Dynamic Spectroscopy, Lichtenbergstraße 4, 85748 Garching, Germany

[2] Institute of Physics, Faculty of Mathematics and Physics, Charles University, Ke Karlovu 5, Prague 121 16, Czech Republic

[3]Department of Chemistry, Ludwig-Maximilians-Universität München, Munich, Germany

Corresponding Author

*juergen.hauer@tum.de

Table of Contents:

Sample preparation

2,10-Bis(1-hexylheptyl)-6-[4′-{2-(3,8,9,10-tetrahydro-9-(1-hexylheptyl)-1,3,8,10-tetraoxoanthra[2,1,9-*def*:6,5,10-*d′e′f′*]diisoquinoline-2(1*H*)-yl]-1*H*-pyrrolo[3′,4′:4,5]pyreno[2,1,10-*def*:7,8,9-*d′e′f′*]diisoquinoline-1,3,5,7,9,11(2*H*,6*H*,10*H*)hexaone: *N*,*N*′-Bis(1-hexylheptyl)benzo[*ghi*]-perylene-2,3,8,9,11,12-hexacarboxylic-2,3:8,9-bis(dicarboximid)-11,12-anhydride (CAS RN 259880-39-2, 110 mg, 130 µmol) and 2-amino-9-(1-hexylheptyl)anthra[2,1,9-*def*;6,5,10-*d'e'f'*]diisoquinoline-1,3,8,10-tetraone (RN 207394-04-5, 100 mg, 170 µmol) were dissolved in quinoline (8 mL) and heated at 150°C for 16 h, allowed to cool, treated with 2 M aqueous HCl (50 mL), extracted with chloroform (3 × 50 mL), dried with magnesiumsulphate, and purified by column separation (silica gel, $CHCl_3$/EtOH 50:1, 600 × 22 mm). Yield 95 mg (52 %) orange red solid, m.p. > 250°C. R_f-value (silica gel, $CHCl_3$/EtOH 50:1) = 0.29. IR (ATR): $\tilde{\nu}$ = 2954.0 (m), 2924.9 (s), 2856.0 (m), 2361.5 (w), 2335.0 (w), 1793.3 (w), 1745.8 (m), 1727.8 (m), 1702.6 (vs), 1662.0 (vs), 1626.2 (w), 1593.8 (m), 1524.7 (w), 1456.6 (w), 1414.4 (m), 1404.3 (w), 1365.3 (m), 1320.9 (vs), 1245.1 (w), 1211.5 (w), 1171.9 (m), 1105.8 (w), 963.9 (w), 852.8 (w), 810.6 (m), 763.1 (w), 749.7 cm^{-1} (w). ^{1}H-NMR (600 MHz, $CDCl_3$, 25°C, TMS): δ = 0.79-0.84 (m, 18 H, 6 × CH_3), 1.21-1.41 (m, 48 H, 24 × CH_2), 1.85-1.96 (m, 6 H, 3 × β-CH_2), 2.23-2.34 (m, 6 H, 3 × β-CH_2), 5.17-5.23 (m, 1 H, N-CH), 5.26-5.32 (m, 2 H, 2 × N-CH), 8.67-8.78 (m, 8 H, 8 × $CH_{perylene}$), 9.20-9.28 (m, 2 H, 2 × $CH_{perylene}$), 9.51 (d, ^3J(H,H) = 8.4 Hz, 2 H, 2 × $CH_{perylene}$), 10.48-10.53 ppm (m, 2 H, 2 × $CH_{perylene}$). ^{13}C-NMR (150 MHz, $CDCl_3$, 25°C, TMS): δ = 14.0, 22.6, 27.0, 29.2, 31.7, 32.4, 54.9, 55.3, 122.2, 123.1, 123.5, 123.9, 124.4, 125.3, 126.1, 126.4, 126.8, 127.0, 127.9, 128.6, 129.5, 130.0, 131.2, 132.7, 133.5, 133.9, 136.2, 160.5, 163.9 ppm. UV/Vis ($CHCl_3$): λ_{max} (ε) = 377.9 (45000), 411.1 (16500), 436.7 (44300), 466.1 (78300), 492.4

(59200), 529.5 nm (95100). Fluorescence ($CHCl_3$, λ_{exc} = 437 nm): λ_{max} (I_{rel}) = 538.8 (1.00), 582.6 (0.51), 632.0 nm (0.12). Fluorescence quantum yield ($CHCl_3$, λ_{exc} = 437 nm, $E_{437\ nm\ /\ 1\ cm}$ = 0.0096, reference: **C25** RN 335458-21-4 with Φ = 1.00): 0.98. MS (FAB^+): *m/z* (%): 1417 (4) [M^+-H], 1236 (14) [M^+], 1055 (15), 1054 (15), 872 (22). $C_{91}H_{95}N_5O_{10}$ (1417.7): Calcd. C 77.04, H 6.75, N 4.94; found C 76.73, H 6.57, N 4.93.

Steady-state spectroscopy

Standard absorption and emission measurements of the BPTI (donor, **D**), PDI (acceptor, **A**) and PBB (dyad, **D-A**) are performed in chloroform at an optical density (OD) of 0.35 at the respective absorption maxima inside a 1 cm cuvette. The absorption spectra are recorded on a UV–VIS spectrophotometer (Lambda 365 UV–VIS spectrophotometer, PerkinElmer Instruments Inc.) and fluorescence spectra are measured on an FS5 spectrofluorometer from Edinburgh Instruments.

Excitation anisotropy

In order to minimize depolarization due to rotational diffusion, all anisotropy measurements were performed on samples dissolved in poly(tetrahydrofuran) (pTHF, average Mn ~2900, Aldrich chemistry). The polymer samples were kept at 30 °C with an electronic Peltier element in order to maintain the transparency of the sample. Excitation anisotropy measurement are performed on the FS5 spectrofluorometer (Edinburgh Instruments) together with two polarizer assemblies, one in the excitation beam path, the other in the emission beam path. Each polarizer assembly contains an α-BBO polarizing prism with an operating range from 220 nm to 900 nm. The rotation of the polarizing prism is computer controlled to an accuracy of 0.5°. An angle of 0° corresponds to vertically linear polarized light, whereas an angle of 90° corresponds to horizontally linear polarized light (vertical and horizontal refer to the optical plane of the FS5 spectrometer). Samples for anisotropy measurement were prepared in poly(tetrahydrofuran) (poly-THF, average $M_n \approx 2900$, Aldrich chemistry) and inside a quartz cuvette with a path length of 1 cm at room temperature, the maximum OD is less than 0.05 to reduce self-absorption. The excitation anisotropy was calculated from

eq. S1
$$r(\lambda_{ex}) = \frac{F_{VV}(\lambda_{ex}) - G(\lambda_{ex}) \cdot F_{VH}(\lambda_{ex})}{F_{VV}(\lambda_{ex}) + 2 \cdot G(\lambda_{ex}) \cdot F_{VH}(\lambda_{ex})},$$

where F represents the fluorescence intensity and the subscripts refer to the settings of the excitation and emission polarizers, respectively. V is the vertical and H the horizontal setting. The $G(\lambda_{ex})$ factor, which is the ratio of the sensitivities of the detection system for vertically and horizontally, is used to corrected the measured spectra and is determined as

eq. S2
$$G(\lambda_{ex}) = \frac{F_{HV}(\lambda_{ex})}{F_{HH}(\lambda_{ex})}.$$

Transient absorption spectroscopy

Femtosecond time-resolved experiments are performed on a home-built transient absorption setup. 800 nm amplified laser pulses (Coherent Legend Elite Duo HE+) with 30 fs (FWHM) temporal duration and a repetition rate of 5 kHz are divided into pump and probe pulses and a temporal delay up to 1.5 ns with a minimum step size

of 15 fs is achieved via optical path length variations using a mechanical delay stage (Newport, M-IMS300C) equipped with a Broadband retroreflector (Newport, M-BBR2.5-0.5). The pump pulse is frequency doubled inside a 100 µm thin beta-barium borate crystal (Bluebean Optical Tech Ltd.) to yield 400 nm excitation pulses with a temporal duration of approx. 54 fs (FWHM) determined from the instrument response function after GLA in OPTIMUS.[1] Its polarization is controlled by a broadband UV (300-470 nm) $\lambda/2$ plate (B.Halle Nachfl. GmbH). 1 µJ pulse is yielded by tuning another broadband visible (600-1200 nm) $\lambda/2$ plate (B.Halle Nachfl. GmbH) before BBO crystal. The pump pulse is focused using a 1 m focal length spherical mirror, and the sample is located in front of the focus where the beam spot size is ~ 1 mm in diameter. White light for detection is generated by focusing the probe laser pulse into a 5 mm thick CaF_2 crystal that is continuously translated in a plane orthogonal to the beam direction, in order to avoid optical damage to the crystal. The focal length is 100 mm and the numerical aperture of the focused beam is chosen to yield a white light spectrum that extends down to 350 nm. The white light pulse is collimated using a 100 mm focal length spherical mirror and the intensity of the fundamental is decreased using a heat absorbing filter. The white light is split into two parts, one part is chosen for probe and another for reference. The probe pulse is focused into the sample by using a 150 mm focal length spherical mirror and the spot size is ~ 100 µm and overlaps with the center of pump, and recollimated by using a 100 mm focal length spherical mirror. The probe and reference laser pulses are detected using a home-built prism spectrometer in combination with a pair of high-speed CMOS linear array cameras (Glaz LineScan-I-Gen2, Synertronic Designs). All the measurements performed in chloroform at an optical density (OD) of 0.3 at the respective absorption maxima at a cuvette with 100 µm optical path length. In addition to **D-A**, the isolated donor molecule was also measured by using same way for comparison. The experiment was done by setting the pump and probe pulses orthogonal, parallel and at MA with each other.

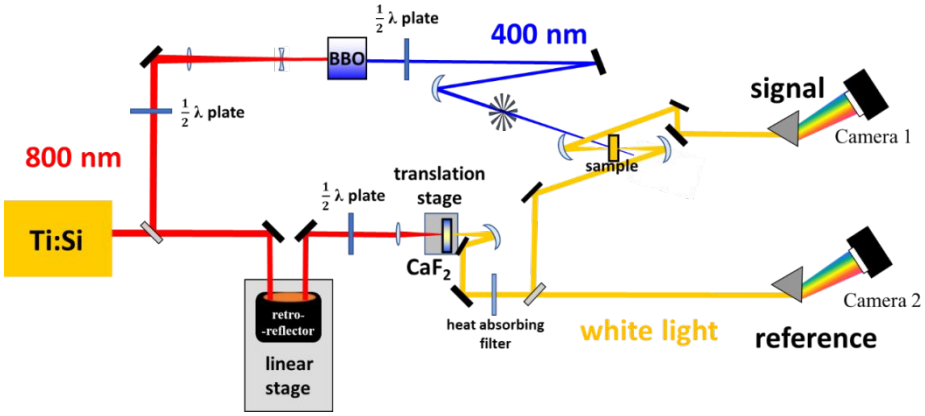

Figure S1 The layout used for polarization-controlled TA experiment

Transient absorption anisotropy spectroscopy

Transient absorption anisotropy spectroscopy (TAA) is obtained by measuring TA spectra for parallel and perpendicular orientation of pump and probe polarizations, $S_{\parallel}(\lambda,t)$ and $S_{\perp}(\lambda,t)$, respectively. This allows to calculate TAA as [2-5]

eq. S3
$$r(\lambda,t) = \frac{S_{\parallel}(\lambda,t) - S_{\perp}(\lambda,t)}{S_{\parallel}(\lambda,t) + 2S_{\perp}(\lambda,t)}.$$

λ and t are written explicitly to highlight the wavelength- and time-dependent nature of the transient signals.

Transient absorption anisotropies (TAA) for both PBB and pure donor were presented in **Fig S4**, traces for each molecule at 435, 510, and 702 nm were plotted. For both dyad and pure donor, the spectral region around 435 nm is dominated GSB of donor. The fact that $r(\lambda,t)$ in this region is constant until 10 ps and then decays due to lack of GSB-signal indicates that rotational diffusion of the molecules is negligible within the observation window of our experiment. Due to energy transfer, the anisotropy trace of the dyad become noisy and lost information after 1 ps, and also cause the anisotropies at 530 and 702 nm in PBB decreased dramatically.

The anisotropy trace of the pure donor keeps steady in the initial 50 ps for all wavelength, which again indicates that rotational diffusion is negligible for this early time window. At 702 nm the ESA transitions is strongest. In absence of energy transfer, we can calculate the ESA-TDM angle β (relative to the GSB-TDM) by using

eq. S4
$$r(\lambda,t) = \frac{2}{5} \cdot \left(\frac{3 \cdot cos^2\beta - 1}{2} \right).$$

This leads to values for β between 42 and 45° at 510 nm, and 30 to 33 ° degree for 702 nm. At 510 nm, we observe two different contributions at early and later times: initially, $r(510nm,t) \approx -0.2$, which speaks for an orthogonal TDM with respect to the GSB's TDM. Hence, we predominantly observe GSB of the acceptor at 510 nm at early times. At later times, $r(510nm,t)$ approaches zero, which is a sign of overall relaxation back to the electronic ground state.

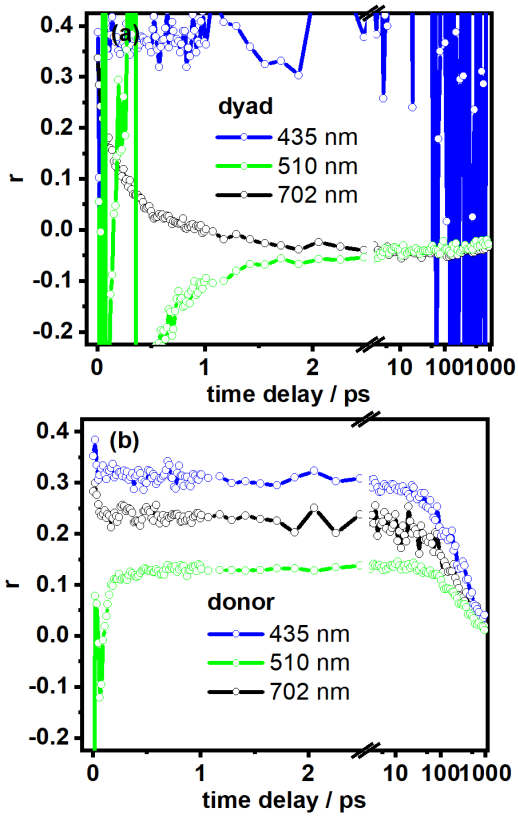

Figure S2 (a) Transient absorption anisotropy spectroscopy (TAA) trances for **(a) D-A** and **(b) D** at 435 nm, 510 nm and 702 nm.

Modification of the S_z and S_y expressions

An experimental set-up is placed in a laboratory Cartesian coordinate system with axes *A*, *B*, and *C*. Light is sent into the sample along the axis *B* and detected in the direction of *C*. The sample consists of randomly oriented, but fixed, molecules with an internal Cartesian axes *X*, *Y*, and *Z*. The polarization of the excitation light will show a component *p* in the direction of *A* and (1-*p*) along *C*. Albrecht showed (see ref. 21 of the main text) that the intensity of light polarized along the laboratory axes is proportional to:

eq. S5
$$I_A \propto (1-p)\, I_B + [3(r_x q_x + r_y q_y + r_z q_z) + q_x(r_y + r_z) + q_y(r_x + r_z) + q_z(r_x + r_y)]$$
$$I_B \propto r_x q_x + r_y q_y + r_z q_z + 2[q(r_y + r_z) + q_y(r_x + r_z) + q_z(r_x + r_y)]$$
$$I_C \propto p\, I_B + (1-p)[3(r_x q_x + r_y q_y + r_z q_z) + q_x\,(r_y + r_z) + q_y(r_x + r_z) + q_z(r_x + r_y)]$$

The factors r_n and q_n refer to absorption and emission along the molecular *n*-axis respectively. In our set-up the exciting light is polarized entirely along the axis *A*-axis - i.e. $p = 1$. We arbitrarily choose the absorption and emission to occur in the molecular *YZ*-plane so that both absorption and emission along *X* is equal to zero, and the expressions above reduce to:

eq. S6
$$I_A = 3(r_y q_y + r_z q_z) + r_y q_z + r_z q_y$$
$$I_B = I_C = r_y q_y + r_z q_z + 2(r_y q_z + r_z q_y)$$

The polarized "unit-vector" spectra can now be constructed by requiring that the absorption from both components sum up to one, i.e.: r_y=1-r_z and r_z=1-r_y. Emission occurs at an angle β, which stands for differences between the TDMs defining the first and last light matter interaction in a TA-sequence induced by thermal fluctuation

eq. S7
$$I_A = (2r_y + 1)\, q_y + (3 - 2r_y)\,(1 - q_y) = (3 - 2\,r_z)\,(1 - q_z) + (2\,r_z + 1)\, q_z$$
$$I_B = I_C = (2 - r_y)\, q_y + (1 + r_y)\,(1 - q_y) = (1 + r_z)\,(1 - q_z) + (2 - r_z)\, q_z$$

These expressions are inserted into the expression for the fundamental anisotropy r_0:

eq. S8
$$r(\lambda,t) = \frac{(I_A - I_B)}{(I_A + I_B + I_C)} = \frac{(I_A - I_B)}{(I_A + 2I_B)}$$
$$= \tfrac{1}{5}\,[(3r_y - 1)\, q_y + (2 - 3\,r_y)\,(1 - q_y)] = \tfrac{1}{5}[(2 - 3\,r_z)\,(1 - q_z) + (3\,r_z - 1)\, q_z]$$

Instead of setting $q_y = 1$ and $q_z = 0$ as ref 6-7, we set $q_y = \cos^2\beta$ and $q_z = \sin^2\beta$. Inserting these requirements into the relevant expressions yields:

eq. S9
$$r_z = \frac{3\cos^2\beta - (2 - 5 \cdot r(\lambda,t))}{3 \cdot (2 \cdot \cos^2\beta - 1)}$$
$$r_y = \frac{3\cos^2\beta - (5 \cdot r(\lambda,t) + 1)}{3 \cdot (2 \cdot \cos^2\beta - 1)}$$

The spectral "unit vectors" along *Y* and *Z* can hence be related directly to the experimentally determined anisotropy $r(\lambda,t)$.

Finally, the purely polarized spectra S_z and S_y can be extracted from the isotropic spectrum $(I_A + 2I_B)$ by projecting it on the appropriate axes using the expressions for the unit vectors above. Using the ordinary notation from polarized spectroscopy, indicating polarizer orientations as either vertical (V) or horizontal (H), the expressions for the purely polarized spectra are:

eq. S10

$$S_z = (S_{\parallel}(\lambda,t) + 2 \cdot S_{\perp}(\lambda,t)) \cdot \left(\frac{3cos^2\beta - (2 - 5 \cdot r(\lambda,t))}{3 \cdot (2 \cdot cos^2\beta - 1)}\right) = 3 \cdot MA \cdot \left(\frac{cos^2\beta - (1 - cos^2\theta)}{(2 \cdot cos^2\beta - 1)}\right)$$

$$S_y = (S_{\parallel}(\lambda,t) + 2 \cdot S_{\perp}(\lambda,t)) \cdot \left(\frac{3cos^2\beta - (5 \cdot r(\lambda,t) + 1)}{3 \cdot (2 \cdot cos^2\beta - 1)}\right) = 3 \cdot MA \cdot \left(\frac{cos^2\beta - cos^2\theta}{(2 \cdot cos^2\beta - 1)}\right)$$

Data analysis: Kinetics

All TA datasets were pre-analyzed by singular value decomposition (SVD) and analyzed by GLA[8] in OPTIMUS.[1] The fitted function includes a sum of 3 to 4 exponentials functions, as well as a combination of Gaussian and Gaussian derivatives to account for the coherent artefact. Evolution-associated spectra (EAS) are obtained based on a sequential kinetic model.

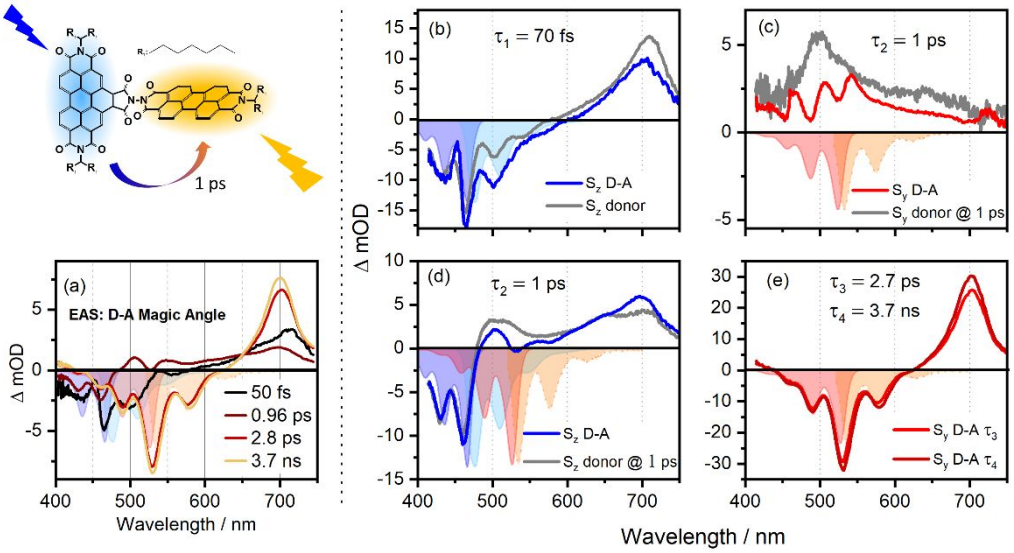

Figure S3 (a) Results from GLA of MA-TA data for **D-A. (b)** the sub-100 fs components of $S_{z-30°}$ retrieved from **D-A** (blue, solid) and **D** (grey, dash dot), **(c)** ~1 ps components of $S_{y-30°}$ for **D-A** (blue, solid) and **D** (grey, dash dot) **(d)** ~1 ps components of $S_{z-30°}$ for **D-A** (red, solid) and **D** (grey, dash dot), and **(e)** the ~ 2.8 ps component of $S_{y-30°}$ (red, solid) and the long-life time component (dark red, solid).

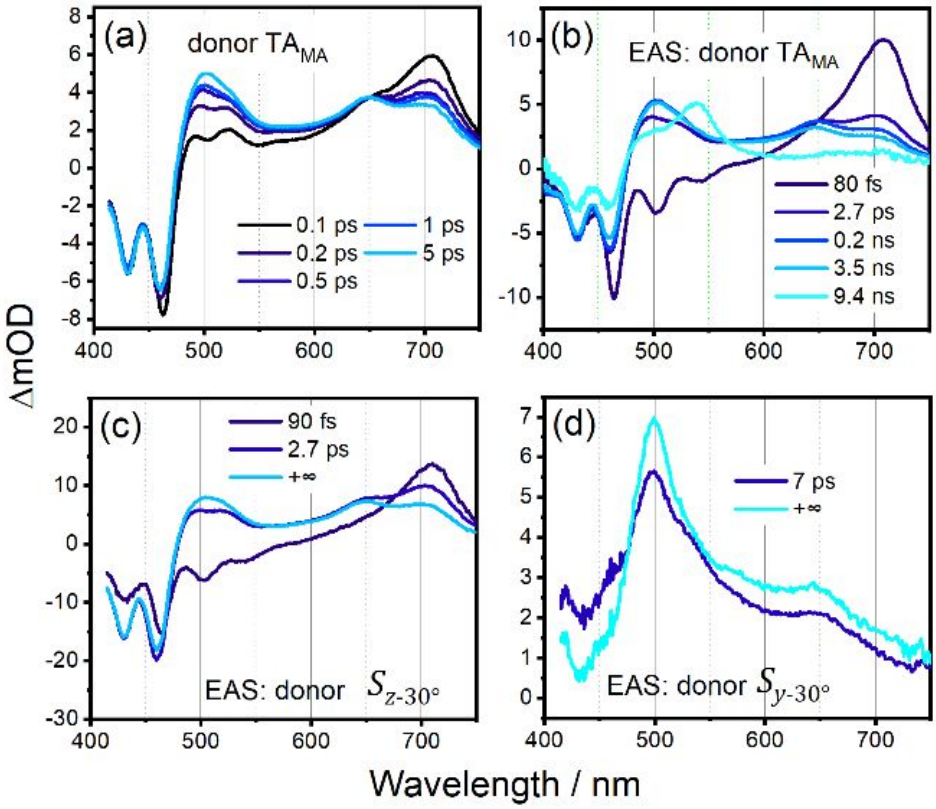

Figure S4 (a) Transient spectra of **D** at indicated delay times, and results from GLA of (b) MA-TA, (c) $S_{z-30°}$ and (d) $S_{y-30°}$ data for **D.**

Table S1 Time constant extracted by global lifetime analysis of MA spectra and corrected spectra of $S_{z-30°}$and $S_{y-30°}$ of BPTI.

	TA_{MA}	$S_{z-30°}$	$S_{y-30°}$
τ_1 **sub-100 fs**	80 fs	90 fs	--
τ_2	2.7 ps	2.7 ps	7 ps*
τ_3*	0.2 ns *	--	--
τ_4	3.5 ns(f)	+∞	--
τ_5	9.4 ns (f)	--	+∞

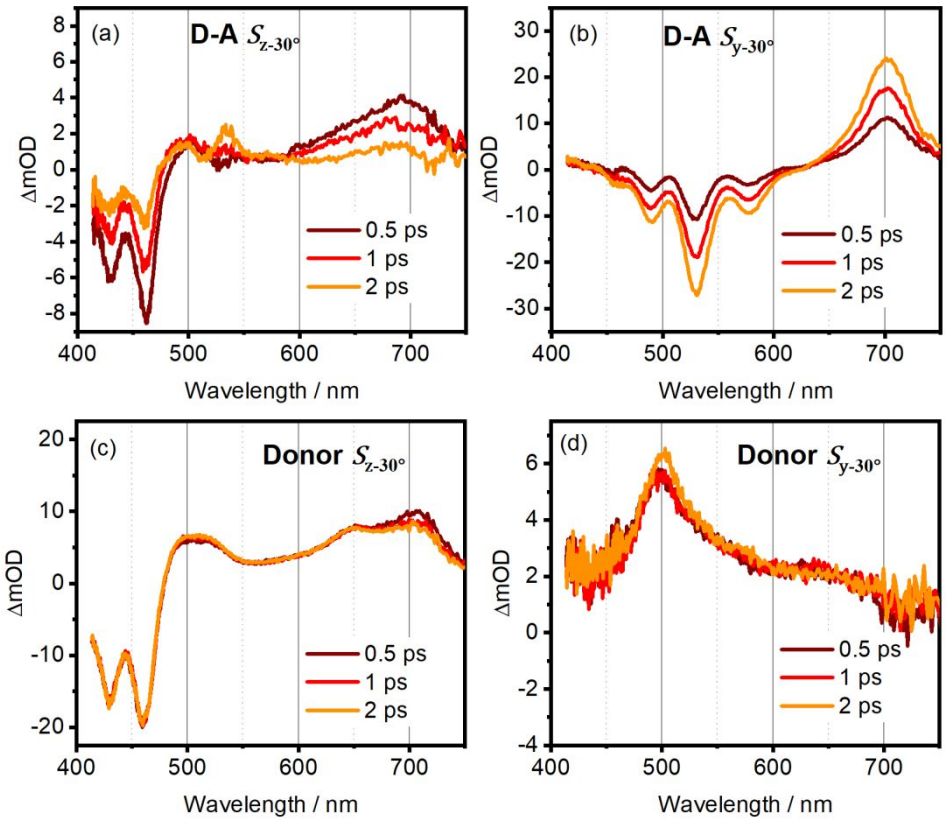

Figure 5 S_z and S_y spectra of **D-A** (top row, (a) and (b)) and **D** (bottom row, (c) and (d)) at 0.5, 1 and 2 ps pump-probe delay. All spectra shown at β values of 30°

QM and MD calculations

All QM calculations are performed using the Gaussian 16 quantum chemistry software.[9] Ground state geometries are optimized with the B3LYP DFT functional and 6-311G(d,p) basis set and the excited state calculations are performed with a long range corrected cam-B3LYP DFT functional[10] and 6-311G(d,p) basis set.[11] Solvent effects were included using a polarizable continuum model (PCM). For computing of the MO overlaps the geometry of the monomers was obtained from the dyad and the missing chemical bond was capped by a hydrogen atom.

Due to the small distance between the donor and acceptor moieties in **D-A** there exists the added possibility of the Dexter type excitation energy transfer.[12] Our computational results, however, indicate that the orthogonal TDMs arrangement of the individual moieties leads to negligible molecular orbital overlap, which is on the order of 4×10^{-4} and 5×10^{-4} for the HOMO and LUMO orbitals, respectively. Overlap between other relevant molecular orbitals is even lower. Such a small molecular orbital overlap yields negligible coupling constants, lower than 0.1 cm^{-1} for Dexter type energy transfer and therefore, even though the donor and acceptor moiety are only separated by a single chemical bond, the geometric arrangement of the moieties leads to negligible molecular orbital overlap and the absence of Dexter type energy transfer.

The orthogonal arrangement of the transition densities of the **D** and **A** in the optimal ground state geometry leads to negligible coupling between the individual moieties. However, the thermal motion of the dyad disrupts the

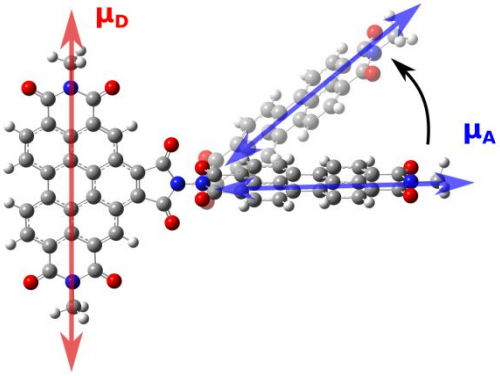

perfect orthogonal arrangement of the transition dipoles of the **D** and **A** moiety and induce coordinate dependent exciton coupling and hence also the excitation energy transfer as was already shown for the dyads with the benzene linker.[11] The major contribution to the coordinate dependent coupling originate from the bending motion of the dyad which leads to the non-orthogonal arrangement of the transition dipole moments of the **D** and **A** moiety. In order to estimate the effect of such molecular motion on the exciton coupling and resulting excitation energy transfer times, the **A** moiety was rotated around the center of the linker in plane defined by **D** moiety (**Figure S6**). For each conformation the transition dipoles were computed for **D** and **A** acceptor moiety separately and placed in the center of charge r_{COC} of each moiety. The center of charge was obtained from integration of the transition density as

eq. S11 $$r_{coc} = \frac{\int r|\rho_{ge}(r)|}{\int|\rho_{ge}(r)|dr},$$

where *r* is electron coordinate and $\rho_{ge}(r)$ is the transition density between the ground and excited state. The exciton coupling *J* between **D-A** was then computed within the point transition dipole approximation as

eq. S12 $$J = \frac{1}{4\pi\epsilon_0}\frac{\mu_{ge}^A \cdot \mu_{ge}^b}{|r_{COC}^A - r_{COC}^B|^3} - 3\frac{\mu_{ge}^A \cdot (r_{COC}^A - r_{COC}^B)\mu_{ge}^B \cdot (r_{COC}^A - r_{COC}^B)}{|r_{COC}^A - r_{COC}^B|^5},$$

where μ_{ge}^A and μ_{ge}^B are transition dipole moments of the acceptor and donor, respectively. The exciton couplings for different mutual angles between the transition dipoles of the **D** and **A** moieties can be found in the Table S2.

Figure S6 The bending motion of the D-A system leads to the non-orthogonal arrangement of the transition dipole moments of the **D** and **A** moiety

Förster energy transfer times estimation

We have recently calculated transfer rates in an ortho-dyad of the same chromophores yet with more distance between D and A, realized by a benzene spacer[11]. After comparing several theoretical approaches, quantitatively accurate estimates were only found only for costly MD/QC simulations, which properly sample both inter- and intra-molecular vibrational motions. In the present work, we limit our efforts to check that the couplings found in Ref [11] rescale correctly for closer arrangement of chromophores with no spacer. Förster energy transfer times were estimated by using the Eq. **(1)** in ref 13 and Eq. **(1)** in ref 14. Using a QM approach described in the previous section, we vary the relative TDM directions of D and A. Results on coupling constant and respective transfer time are shown in Table S2. For the ortho-FRET system including the benzene spacer, the observed EET-time of 9.4 ps, corresponding to an angle of $67°$.[13] Applied to the present nullspacer dyad, the Förster rate is calculated to be 1.6 ps, see table S2. This compares well to our experimental finding of 0.96 ps . From other point of view the

nullspacer lifetime correspond to 61° angle between donor and acceptor dipoles as reported in the main text. We conclude that both spectra and transport data qualitatively support the picture of Förster type of transport, but the estimate of orientation factor for Förster formula remains challenging.

Table S2 Förster energy transfer times of D-A system with and without benzene spacer estimated by dipole-dipole approximation. The coupling values obtained by MD method with different angle between TDMs of donor and acceptor.

Spacer	Angle between TDM of D and A / °	Coupling (dip-dip)/ cm^{-1}	Life time estimated / ps
Benzene	76	10.62	25.62
	72	13.68	15.44
	68	16.82	10.21
	64	20.07	7.17
	60	23.45	5.25
	56	27.00	3.96
	52	30.71	3.06
	48	34.65	2.41
Null	76	24.97	4.63
	72	32.61	2.72
	68	40.47	1.76
	64	48.60	1.22
	60	57.06	0.89
	56	65.93	0.66
	52	75.28	0.51
	48	85.18	0.40

REFERENCES

(1) Slavov, C.; Hartmann, H.; Wachtveitl, J. Implementation and Evaluation of Data Analysis Strategies for Time-Resolved Optical Spectroscopy. *Anal. Chem.* **2015,** *87* (4), 2328-36, DOI: 10.1021/ac504348h.

(2) Jonas, D. M.; Lang, M. J.; Nagasawa, Y.; Joo, T.; Fleming, G. R. Pump−Probe Polarization Anisotropy Study of Femtosecond Energy Transfer within the Photosynthetic Reaction Center of Rhodobacter Sphaeroides R26. *J. Phys. Chem.* **1996,** *100* (30), 12660-12673, DOI: 10.1021/jp960708t.

(3) Yeh, A. T.; Shank, C. V.; McCusker, J. K. Ultrafast Electron Localization Dynamics Following Photo-Induced Charge Transfer. *Science* **2000,** *289* (5481), 935-8, DOI: 10.1126/science.289.5481.935.

(4) Mewes, L.; Ingle, R. A.; Megow, S.; Böhnke, H.; Baranoff, E.; Temps, F.; Chergui, M. Ultrafast Intersystem Crossing and Structural Dynamics of [Pt (Ppy)(M-T Bu2pz)] 2. *Inorg. Chem.* **2020,** *59* (20), 14643-14653, DOI: 10.1021/acs.inorgchem.0c00902.

(5) Wallin, S.; Davidsson, J.; Modin, J.; Hammarstrom, L. Femtosecond Transient Absorption Anisotropy Study on [Ru(Bpy)3]2+ and [Ru(Bpy)(Py)4]2+. Ultrafast Interligand Randomization of the Mlct State. *J. Phys. Chem. A* **2005,** *109* (21), 4697-704, DOI: 10.1021/jp0509212.

(6) Thyrhaug, E.; Zidek, K.; Dostal, J.; Bina, D.; Zigmantas, D. Exciton Structure and Energy Transfer in the Fenna-Matthews-Olson Complex. *J. Phys. Chem. Lett.* **2016,** *7* (9), 1653-60, DOI: 10.1021/acs.jpclett.6b00534.

(7) Thyrhaug, E.; Sorensen, T. J.; Gryczynski, I.; Gryczynski, Z.; Laursen, B. W. Polarization and Symmetry of Electronic Transitions in Long Fluorescence Lifetime Triangulenium Dyes. *J. Phys. Chem. A* **2013,** *117* (10), 2160-8, DOI: 10.1021/jp312376k.

(8) Landl, G.; Langthaler, T.; Englt, H. W.; Kauffmann, H. F. Distribution of Event Times in Time-Resolved Fluorescence: The Exponential Series Approach—Algorithm, Regularization, Analysis. *J. Comput. Phys.* **1991,** *95* (1), 1-28, DOI: 10.1016/0021-9991(91)90250-O.

(9) Frisch, M. J.; Trucks, G. W.; Schlegel, H. B.; Scuseria, G. E.; Robb, M. A.; Cheeseman, J. R.; Scalmani, G.; Barone, V.; Petersson, G. A.; Nakatsuji, H., et al. *Gaussian 16 Rev. A.03*, Wallingford, CT, 2016.

(10) Yanai, T.; Tew, D. P.; Handy, N. C. A New Hybrid Exchange–Correlation Functional Using the Coulomb-Attenuating Method (Cam-B3lyp). *Chem. Phys. Lett.* **2004,** *393* (1-3), 51-57, DOI: 10.1016/j.cplett.2004.06.011.

(11) Slama, V.; Perlik, V.; Langhals, H.; Walter, A.; Mancal, T.; Hauer, J.; Sanda, F. Anharmonic Molecular Motion Drives Resonance Energy Transfer in Peri-Arylene Dyads. *Front. Chem.* **2020,** *8*, 579166, DOI: 10.3389/fchem.2020.579166.

(12) Dexter, D. L. A Theory of Sensitized Luminescence in Solids. *J. Chem. Phys.* **1953,** *21* (5), 836-850, DOI: 10.1063/1.1699044.

(13) Renger, T.; Dankl, M.; Klinger, A.; Schlucker, T.; Langhals, H.; Muh, F. Structure-Based Theory of Fluctuation-Induced Energy Transfer in a Molecular Dyad. *J. Phys. Chem. Lett.* **2018,** *9* (20), 5940-5947, DOI: 10.1021/acs.jpclett.8b02403.

(14) Langhals, H.; Dietl, C. Vibronic Intramolecular Resonant Energy Transfer Along More Than 5 Nm: Synthesis of Dyads for a Re-Examination of the Distance Function of Fret. *J. Org. Chem.* **2022,** *87* (15), 9454-9465, DOI: 10.1021/acs.joc.1c02682.